

Adaptive slicing based on efficient profile analysis

Mao, Huachao ; Kwok, Tsz-Ho; Chen, Yong; Wang, Charlie C.L.

DOI

[10.1016/j.cad.2018.09.006](https://doi.org/10.1016/j.cad.2018.09.006)

Publication date

2019

Document Version

Final published version

Published in

CAD Computer Aided Design

Citation (APA)

Mao, H., Kwok, T.-H., Chen, Y., & Wang, C. C. L. (2019). Adaptive slicing based on efficient profile analysis. *CAD Computer Aided Design*, 107, 89-101. <https://doi.org/10.1016/j.cad.2018.09.006>

Important note

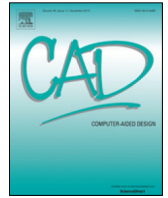
To cite this publication, please use the final published version (if applicable).
Please check the document version above.

Copyright

Other than for strictly personal use, it is not permitted to download, forward or distribute the text or part of it, without the consent of the author(s) and/or copyright holder(s), unless the work is under an open content license such as Creative Commons.

Takedown policy

Please contact us and provide details if you believe this document breaches copyrights.
We will remove access to the work immediately and investigate your claim.



Adaptive slicing based on efficient profile analysis

Huachao Mao^a, Tsz-Ho Kwok^a, Yong Chen^{a,*}, Charlie C.L. Wang^b

^a Epstein Department of Industrial and Systems Engineering, University of Southern California, Los Angeles, CA 90089, USA

^b Department of Design Engineering, Delft University of Technology, The Netherlands



ARTICLE INFO

Article history:

Received 9 July 2016

Accepted 29 September 2018

Keywords:

Additive manufacturing

Adaptive slicing

Geometric profile

Sampling

ABSTRACT

Adaptive slicing is an important computational task required in the layer-based manufacturing process. Its purpose is to find an optimal trade-off between the fabrication time (number of layers) and the surface quality (geometric deviation error). Most of the traditional adaptive slicing algorithms are computationally expensive or only based on local evaluation of errors. To tackle these problems, we introduce a method to efficiently generate slicing plans by a new metric profile that can characterize the distribution of deviation errors along the building direction. By generalizing the conventional error metrics, the proposed metric profile is a density function of deviation errors, which measures the global deviation errors rather than the in-plane local geometry errors used in most prior methods. Slicing can be efficiently evaluated based on metric profiles in contrast to the expensive computation on models in boundary-representation. An efficient algorithm based on dynamic programming is proposed to find the best slicing plan. Our adaptive slicing method can also be applied to models with weighted features and can serve as the inner loop to search the best building direction. The performance of our approach is demonstrated by experimental tests on different examples.

© 2018 Elsevier Ltd. All rights reserved.

1. Introduction

Over the last thirty years, a new type of manufacturing process, called additive manufacturing (AM), has been developed using the principle of layer-based material accumulation [1]. Many novel AM processes based on different techniques such as laser curing, nozzle extrusion, jetting, electron beam, and laser cutter, have been developed [2]. AM is a direct manufacturing process that can fabricate parts directly from *computer-aided design* (CAD) models without part-specific tools or fixtures. Therefore, it can fabricate highly complex parts effectively. In most of the AM processes, the digital CAD model is sliced by intersecting it with a number of horizontal planes. The sliced contours are then transferred to generate the tool paths for material accumulation. While the uniform layer thickness is widely used due to its simplicity, it has been theoretically proven that adaptive layer thickness can produce parts with higher accuracy and shorter building time [3,4]. In adaptive slicing, the varied thickness of layers is determined by the geometry of input models. Most of the existing methods [4] evaluate deviation errors locally by the geometry at particular slicing planes, which can result in large approximation error when there is complex geometry between neighboring slices.

To improve the accuracy of geometry error evaluation, different strategies have been developed, including: (1) slicing the model

using the finest layer thickness [5], (2) direct slicing the designed CAD model (like NURBS [6], CSG [7]) rather than the related tessellated model (like STL [3]), and (3) refining the slicing plan if sharp geometry changes are detected within one layer [8]. However, these methods are computationally expensive, and the bottleneck is caused by the process requiring a large number of intersection operations between the slicing plane and the CAD model.

In this paper, we develop a novel method to overcome this bottleneck by representing a CAD model as a profile of the geometric error along the building direction. An example is shown in Fig. 1. The evaluation of the geometric deviation error can be done on the profile rather than intersecting the CAD model intensively. By constructing the metric profiles using GPU-accelerated methods, the whole process of adaptive slicing can be computed in about one second. In summary, our presented adaptive slicing technique is accurate and efficient. The main contribution is a new profile-based framework for adaptive slicing, which shows the following properties.

- Global:** The profile generalizes the conventional error metrics and provides an implicit representation for the shape of an input model, and it is global information for slicing. Based on that, we design an optimization algorithm based on dynamic programming to find the best slicing plan.
- Efficient:** The analysis taken in our algorithm is based on a metric profile that can be generated by GPU-accelerated techniques. In our tests, the whole process from profile

* Corresponding author.

E-mail address: yongchen@usc.edu (Y. Chen).

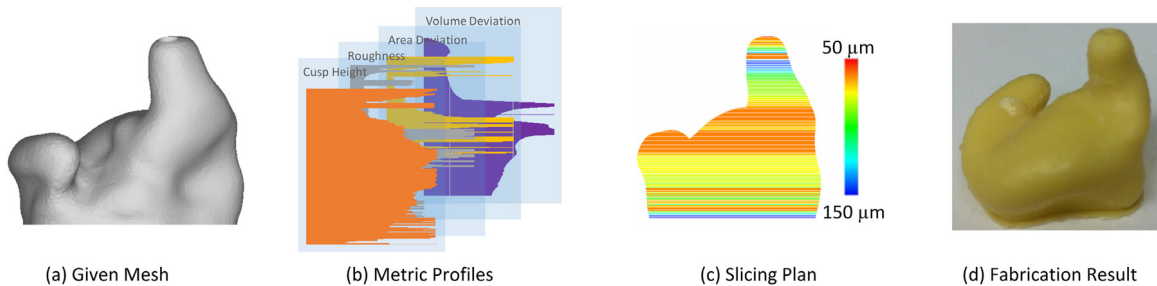


Fig. 1. Given a mesh model with weights on faces (a), the metric profiles (b) are extracted to describe the surface metric distributions along a building direction. Based on these profiles and the mesh weight, an optimal slicing plan (c) can be computed. The color scale in (c) represents the layer thickness value, and the smaller the layer thickness is, the color is closer to the red end. And all the figures in this paper share this same color scale for layer thickness. The result of the model fabricated by the optimal slicing is shown in (d), and the comparisons can be found in Fig. 10. (For interpretation of the references to color in this figure legend, the reader is referred to the web version of this article.)

construction to getting the optimal slicing plan can be completed in around one second. Benefiting from the efficiency, it can serve as the inner loop to find the best building direction.

- General:** The formulation can be easily extended to integrate different commonly used error metrics. Moreover, we also show that it can be further generalized to incorporate the user specified salience.

The rest of the paper is organized as follows. Section 2 briefly describes the related work of adaptive slicing in additive manufacturing. After that, the details of our framework are given in Section 3. Section 4 demonstrates the generality of the presented framework by considering different factors. Results and statistics are given in Section 5, and our paper ends with conclusions and discussions in Section 6.

2. Related work

Layer-based additive manufacturing fabricates a part by successively accumulating material layer by layer, in which an essential computational step is slicing. In the step of slicing, the input CAD model is intersected with a set of horizontal planes, and this results in a set of closed curves or polygons at different height levels. Assuming each layer is fabricated by extruding the intersected contour with a small layer thickness, such an extrusion introduces the staircase error [9], which is directly related to the surface angle and the layer thickness [10]. Slicing methods can be classified into uniform (having an equal thickness in all layers) or adaptive ones (with unequal layer thicknesses in different layers). While uniform slicing is simple and fast, adaptive slicing is proven to be able to fabricate parts with higher accuracy and shorter building time.

2.1. Surface quality

Various slicing procedures have been discussed in previous surveys of AM technology [11,12], where the resultant quality is measured by different geometric errors – e.g., cusp height, surface roughness (Ra), and area or volumetric deviation. The most widely used error measurement is the cusp height [3]. Kulkarni and Dutta [4] reduced the staircase effect by controlling the maximum allowable cusp height using 12 different expressions. The relationship between the maximal allowed cusp height and the normal vector at any point on the tessellated model is used to find the thickness of each layer. Yan et al. [13,14] followed this idea and developed an adaptive slicing method that works directly on point cloud by using moving least square surfaces. This error measurement has also been used widely in different applications [15–19]. Recently, Wang et al. [20] presented an adaptive slicing method considering both the cusp height and saliency criterion. The Ra

value [8], which is commonly used in design or manufacturing practice to specify surface roughness, is a similar measurement that can be used as well. Differently, Zhao [7] introduced area deviation by comparing the measured deviation of the interior area of the layer contours to check whether the layer becomes thicker or thinner. However, a staircase effect appears on the layer while two contours have a similar area but totally different shapes. All of these errors can be classified as 2D measurements. They become less suitable when the geometry of an input model between two neighboring slices becomes more complex. To address the problem, Kumar and Choudhury [21] presented a volume deviation for adaptive slicing. This technique is a promising solution for slicing CAD models with remarkable higher precision. However, since it works directly with surfaces of the part to mathematically compute the related volumes, the geometric complexity of the surfaces would need some complicated mathematical computation that may jeopardize the validity of such system.

2.2. Global slicing

Most of the previous work (e.g., [22]) first cuts the entire part from the bottom-most to the top-most position at the maximal thickness that is allowed by the AM process, and then applied the specific error to decide if some thicker layers need to be further sliced into thinner ones. However, the presence of any concave or convex area may yield a significant geometry deviation error when no staircase effect is identified at either slicing layers. In contrast, Hayasi and Asiabanpour [5] started slicing at the minimal allowed thickness, then allowed the current layer becomes thicker or thinner while comparing the obtained error with the given tolerance. Singhal et al. [8] presented a comprehensive and more accurate direct slicing procedure by detecting the sharp concave/convex vertices and then subdividing a large layer into a number of thinner layers if sharp concave/convex vertices are detected. Wang et al. [20] proposed an iterative method to refine the slicing plan obtained by previous greedy methods. All these slicing procedures are trying to obtain the geometry's sharp changes as accurately as possible, either by cutting at minimum thickness or by checking the sharp vertices. However, the expensive computation prevents to applying this methodology at very high resolution. To solve this dilemma, we introduce a slicing algorithm that optimizes the slicing plan on a profile, which can be efficiently constructed from the CAD model.

3. Adaptive slicing based on metric profiles

The complexity of the slicing optimization problem mainly arises from the evaluation of geometry error. This geometry error calculation is time consuming because most slicing algorithms are based on NURBS [6], STL [3] or point cloud set [14], and slicing

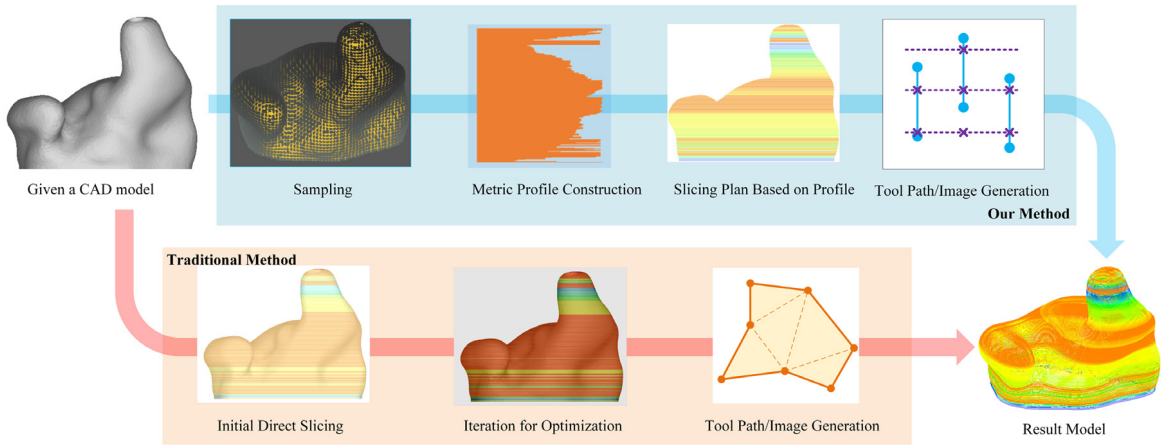


Fig. 2. Comparison between the traditional and our newly proposed adaptive slicing pipelines.

one 3D model based on these representations is computationally expensive. Instead of directly evaluating the deviation error on input CAD models, we propose an intermediate *metric profile* to evaluate the deviation error distribution along the z axis (the printing direction). The value of metric profile $\phi(z)$ is a measure of geometric error density with reference to the height z . Based on the definition of metric profile $\phi(z)$, we can evaluate both the error metric of each layer and the total error with trivial effort. Specifically, the metric error ε_k of a layer k is defined as the integral of a metric profile function along that layer's height range $[z_{k-1}, z_k]$ as

$$\varepsilon_k = \int_{z_{k-1}}^{z_k} \phi(z) dz, \quad (1)$$

Problem Definition: Based on the metric profile (error density function) $\phi(z)$ and given the allowed maximal error ϵ of a layer, the optimization objective is to minimize the total number of layers while assuring each layer's integral error ε_k is within the given tolerance ϵ , i.e.

$$\begin{aligned} \min \quad & K \\ \text{s.t.} \quad & \varepsilon_k = \int_{z_{k-1}}^{z_k} \phi(z) dz \leq \epsilon, k = 1, \dots, K \quad (C1) \\ & z_k = z_{k-1} + t_k, k = 1, \dots, K \quad (C2) \\ & t_{\min} \leq t_k \leq t_{\max}, k = 1, \dots, K \quad (C3) \\ & z_0 = 0, z_K = H, \quad (C4) \end{aligned} \quad (2)$$

where $\phi(z)$ is the metric profile function, the unknown variable K is the number of layers, the unknown variable t_k is the thickness of layer k , t_{\min} and t_{\max} are the manufacturing constraints of the minimal and maximal layer thickness, and H is the height of the input model.

To solve this slicing problem, we propose a novel adaptive slicing pipeline as shown in Fig. 2. Different from the traditional adaptive slicing pipeline that directly performs the slicing on the CAD model (refer to the bottom row of Fig. 2), our new pipeline first efficiently samples the input 3D model into structured points and then constructs the metric profile from the sampled points. Using the metric profile, we can efficiently obtain the optimal slicing plan, and eventually export the tool paths for 3D printers such as Fused Deposition Modeling (FDM) [23] or projection-based Stereolithography (SLA) [24]. The details of each step in our new framework will be discussed as follows.

3.1. Metric profile

We introduce “metric profile” $\phi(z)$ to describe the geometry error distribution along the z direction (the printing direction). The

metric profile is a function to measure the geometry error density at height z . There are different error metrics that can be used to construct the profile as discussed in Section 2.1, e.g., cusp height, surface roughness, area deviation and volume deviation. The proposed framework is compatible and useful for all these errors and other applications as long as a metric profile can be defined. In this section, as a widely used metric since its development [3], the cusp height is picked to explain the algorithm. In Section 4.1, we will demonstrate that a similar setting can be developed for other error metrics, as well as the weighted saliency $\omega(z)$ in Section 4.2.

The error metric “cusp height” is to measure geometry error due to the lack or surplus of materials caused by slicing. The cusp height c of the i th layer is calculated by its thickness t_i and the normal of the points in the layer. Assume the slicing is along the z direction and the maximum value of normal in z -axis is n_z (from a normal vector $\mathbf{n} = (n_x, n_y, n_z)$), the cusp height of the layer can be approximated by

$$c = \|t_i \cdot n_z\|_{\infty}. \quad (3)$$

As there are many points with different normal values in a layer, the infinity norm is used (i.e., the maximum value of n_z is picked as the error density) to conservatively preserve the sharpest feature. Remark that, the metric of cusp height is used here just for the sake of explaining the algorithm, but same concepts can be applied to other metrics.

By definition, the thickness t_i is always along the printing direction z , so a change in the value of t_i can be denoted as Δz . Thus the corresponding change in cusp height is $\Delta c = \Delta z \|n_z\|_{\infty}$. Therefore, the metric profile for cusp height is defined as the derivative of c w.r.t. the height z :

$$\phi_{\text{cusp}}(z) = \frac{dc}{dz} = \lim_{\Delta z \rightarrow 0} \frac{\Delta c}{\Delta z} \approx \max\{n_z\}. \quad (4)$$

Based on the above-defined error metric profile, we can easily calculate the metric error ε_k of a layer k within the height range $[z_{k-1}, z_k]$ as the integral of metric profile $\varepsilon_k = \int_{z_{k-1}}^{z_k} \phi(z) dz$. Noted that, this proposed integral error metric is a generalization of the conventional slicing algorithm using cusp height. The illustration and comparison of the approximation errors between the conventional and the proposed methods are given in the Appendix. In Section 4.1, we will see the concept of “metric profile” could be extended to other commonly used geometry error metrics, such as surface roughness, area deviation and volume deviation.

3.2. Sampling for profile construction

To improve the efficiency of the implementation, the entire range of the metric profile $\phi(z)$ is divided into a series of intervals.

The bins (intervals) are consecutive and non-overlapping intervals of the height z , and they have equal size of b , i.e., $\phi(z) = \{\tilde{\phi}(1), \dots, \tilde{\phi}(N)\}$ where $N = \lceil \text{model height}(H)/\text{interval size}(b) \rceil$ is the number of bins, and the size of each interval b is set as a small value (2 μm in our test cases; in comparison, the layer thickness typically used in SLA is 100 μm , and the choice of b will be discussed in Section 5). We employ the sampling techniques to facilitate the computation of the metric profile value in each interval. It can be well-structured points, voxels, or rays, and the geometric error could be easily evaluated by checking all the sampled points falling into the corresponding interval. This process is efficient compared to the expensive intersection operation based on the original CAD model.

In this paper we choose the Layer Depth Image (LDI) as our sampling approach. LDI [25–27] is an extension of the ray representation (ray-rep) in solid modeling. Based on a well-structured discrete sampling approach, LDIs can efficiently and robustly perform a set of complex geometric operations, including off-setting [28,29], Boolean [30], regulation [31] and overhang area evaluation [32]. By parallel GPU computing, LDI could achieve high resolution efficiently (a STL model with 1 million faces can be sampled into LDI within one second). Comparing to directly slicing a model with similar complexity in the finest resolution that takes several minutes, it saves a lot of computation time. Generally, the resolution of the LDI is dense enough for normal models. For a bigger size model or a higher accuracy is needed, a technique called volume tiling [31] can be used. That is, the bounding box of a model is first split into smaller tiles. Each tile is then processed independently and we construct their LDI models respectively. Besides the sampling efficiency, LDI is also a rich sampling representation (denoting a sampled model as $P = \{p_j\} = \{x_j, y_j, z_j, n_j^x, n_j^y, n_j^z, f_j, r_j\}$), which includes the point coordinate (x_j, y_j, z_j) , normal (n_j^x, n_j^y, n_j^z) , ID of facet f_j where the point belongs to, and ID of sampling ray r_j that has the information of point adjacency and In/Out specification (i.e., the intersection point where the ray goes into or gets out from the model).

Among the information, the point coordinate (x_j, y_j, z_j) is always useful, and the facet ID f_j is used to retrieve the weight ω_j . In addition, the normal (n_j^x, n_j^y, n_j^z) is used to construct the profiles of “cusp height” and “surface roughness”, while the ID of sampling ray r_j is used to build the profiles of “area deviation” and “volume deviation”. The ray r_j is also useful in the generation of toolpaths/mask-images for fabrication.

For example, the cusp metric profile in eq.(4) requires the normal (n_j^x, n_j^y, n_j^z) . The construction of the metric profile can be performed efficiently by grouping the points into the corresponding intervals according to their heights. Recall that the metric profile of cusp height in Eq. (4) is discretized into N intervals, and for each interval i , the metric value $\tilde{\phi}_{\text{cusp}}(i)$ is the maximal value of n_z among all the points inside the interval, i.e.,

$$\tilde{\phi}_{\text{cusp}}(i) = \max \{n_j^z | \lceil z_j/b \rceil = i, P_j \in P\}, \quad (5)$$

Hence, the metric profile value at height z could be approximated as

$$\tilde{\phi}_{\text{cusp}}(z) \approx \tilde{\phi}_{\text{cusp}}(\lceil z/b \rceil). \quad (6)$$

This profile construction process can be done within 50 ms on GPU for all our tests.

Section 4.1 will introduce some other metric profiles, which can also be constructed using the LDI information, and the detailed usage will be discussed there.

3.3. Slicing algorithm

After constructing the metric profile $\phi(z)$, we have all the information to formulate the slicing optimization problem of Eq. (2). We

Metric Profile	$\tilde{\phi}(1)$ 0.2	$\tilde{\phi}(2)$ 0.2	$\tilde{\phi}(3)$ 0.2	$\tilde{\phi}(4)$ 0.3	$\tilde{\phi}(5)$ 0.4	$\tilde{\phi}(6)$ 0.1	$\tilde{\phi}(7)$ 0.2	$\tilde{\phi}(8)$ 0.2	
SP#	0	1	2	3	4	5	6	7	8
$K[i]$	0	∞	1	1	2	∞	3	∞	4
$D[i]$	NA	NA	0	0	2	NA	4	NA	6
$S[i]$	True	False	True	False	True	False	True	False	True

Fig. 3. An example with the first 8 intervals in the metric profile is used to illustrate the Dynamic Programming based slicing process. SP# — slice plane number, $S[i]$ — the resulted optimal slicing plan.

represent the slicing plan (S) as a boolean array with a size equal to the number of intervals $N + 1$, where the value of *true* or *false* stands for if there is a slice on that particular height or not. There are manufacturing constraints of the minimal and maximal layer thickness $[t_{\min}, t_{\max}]$, and the size of interval b . As the intervals are used to optimize the location of the slicing planes, if b is a common factor of t_{\min} and t_{\max} , it is possible for the algorithm to utilize the whole range of layer thickness. Otherwise, the range of the layer thickness will be narrowed down, and the minimal and maximal number of intervals in one layer will be $\lceil t_{\min}/b \rceil$ and $\lfloor t_{\max}/b \rfloor$.

To find a slicing plan, one may apply a greedy algorithm to assign as many intervals as possible to a layer until the sum of metric profile $\tilde{\phi}(i)$ exceeds the tolerance ϵ . However, a greedy heuristic may yield locally optimal solutions and fail to satisfy the constraints while the minimal layer thickness is restricted. Although it is faster to calculate, we find that this kind of situation is not rare and appears from time to time. Moreover, such a greedy algorithm cannot guarantee the result with a minimal number of layers. It motivated us to design an efficient algorithm based on Dynamic Programming (DP) [33] to compute a true global optimum. For a bottom-to-top DP algorithm, it starts from the head and computes sub-solutions from smaller to bigger problems, and then stores the intermediate results in the memory. These previously computed solutions are combined to give the best solution for the whole problem. Once it has reached the tail, the optimal slicing plan can be extracted by backtracking.

The process is illustrated using an example of first 8 intervals $\{\tilde{\phi}(1), \dots, \tilde{\phi}(8)\}$ shown in Fig. 3. Assume the allowable error of a layer is $\epsilon = 0.6$, and the minimal and maximal number of intervals in a layer are 2 and 3 to satisfy the constraint C3 in Eq. (2), i.e., $\lceil t_{\min}/b \rceil = 2$ and $\lfloor t_{\max}/b \rfloor = 3$. A weight array $K[0 \dots 8]$ and an index array $D[0 \dots 8]$ for the slicing planes, i.e., $K[1]$ is in between $\tilde{\phi}(1)$ and $\tilde{\phi}(2)$. The weight array $K[\dots]$ stores the least number of layers and the index array $D[\dots]$ records the index of optimal slicing positions, which will be used in backtracking.

Starting from the head (0th), it is initialized with $K[0] = 0$ and $D[0] = \text{NA}$ as the first slice plane to satisfy C4 in Eq. (2). The 1st-plane is initialized with $K[1] = \infty$ and $D[1] = \text{NA}$ as for the minimal number of intervals to form a layer is 2, it is not allowed to put a slice plane here. For the 2nd-plane, it can form a layer only with 0th-plane including $\tilde{\phi}(1)$ and $\tilde{\phi}(2)$, so $K[2] = K[0] + 1 = 1$, where the ‘+1’ means one layer, and $D[2] = 0$, meaning 0th-plane. In other words, if there is a slice plane on 2nd-plane, this layer is optimal forming by the 0th-plane and itself. As the minimal and maximal number of intervals are 2 and 3, there are two possible positions to form a layer with the 3rd-plane, which are the 0th- and 1st-plane. A comparison can be made to find the optimal one, and this sub-solution will be stored in the memory. Specifically, two cases of forming a layer with the 0th-plane including $\tilde{\phi}(1)$ to $\tilde{\phi}(3)$ and with 1st-plane including $\tilde{\phi}(2)$ to $\tilde{\phi}(3)$ are compared, and the minimum one is picked. For 0th-plane, it is $K[0] + 1 = 1$; and for 1st-plane, it is $K[1] + 1 = \infty + 1 = \infty$. In this case the 0th-plane wins, and this sub-solution is stored as $K[3] = 1$ and $D[3] = 0$. Similarly, the 4th-plane will store $K[4] = 2$ and $D[4] = 2$. For the

5th-plane, the two cases are with the 3rd-plane and the 4th-plane. However, both $\tilde{\phi}(3) + \tilde{\phi}(4) + \tilde{\phi}(5) = 0.9$ and $\tilde{\phi}(4) + \tilde{\phi}(5) = 0.7$ exceeds the allowable error of a layer $\epsilon = 0.6$. Therefore, none of them is feasible, so the weight is set as $K[5] = \infty$ and $D[5] = NA$ to prevent a plane is placed at this position. The iteration continues, and the rest are $K[6] = 3$ and $D[6] = 4$; $K[7] = \infty$ and $D[7] = NA$; $K[8] = 4$ and $D[8] = 6$.

The key of the DP algorithm is making use of the stored sub-solutions (e.g., $K[0 \dots 7]$) to compute the later ones until the last ($K[8]$). Once it has been done, the optimal slice plan can be extracted by backtracking using the index array $D[0 \dots 8]$. Starting from $D[8]$, which records the optimal one to form a layer should be the 6th-plane, and recursively $D[6]$ returns 4, $D[4]$ returns 2, and $D[2]$ returns 0, which reaches the head. As a result, the slice plan $S[0] = S[2] = S[4] = S[6] = S[8] = True$, and there are four layers: $(\tilde{\phi}(1) \tilde{\phi}(2))$, $(\tilde{\phi}(3) \tilde{\phi}(4))$, $(\tilde{\phi}(5) \tilde{\phi}(6))$, and $(\tilde{\phi}(7) \tilde{\phi}(8))$. The slice plan is valid and each of the layers has an error smaller than the allowable error, so the DP algorithm can find a global optimum where the greedy algorithm probably will take the first three intervals $(\tilde{\phi}(1) \tilde{\phi}(2) \tilde{\phi}(3))$ and get a local optimum for the first layer, and then being stuck with $(\tilde{\phi}(4) \tilde{\phi}(5))$ as the sum of them (0.7) is greater than the allowable error $\epsilon = 0.6$.

Note that, if there is no feasible solution, the tail will store invalid values, e.g., $K[8] = \infty$ and $D[8] = NA$, and the system will report and ask for a revision of the constraints. Otherwise, the backtracking will never reach the head.

A general version of the slicing algorithm is summarized in Procedure 1. It takes a linear time $O(N)$ to compute and track the optimal slicing plan, where N is the number of intervals (the worst case is quadratic time $O(N^2)$ for the range of minimal and maximal interval number in a layer equals to the total number of intervals). In all of our test cases, this slicing algorithm takes less than 5 ms.

Procedure 1: Slicing Based on Dynamic Programming.

Input: Metric profile intervals $\{\tilde{\phi}(1), \dots, \tilde{\phi}(N)\}$, interval size b , allowable error for a layer (ϵ), max/min layer thickness (t_{min}, t_{max})

Output: Slicing Plan $S[0 \dots N]$

```

//initialization
1:  $S[0 \dots N] = false$ ;  $K[0 \dots N] = \infty$ ,  $D[0 \dots N] = NA$ 
2:  $K[0] = 0$ ; //for the 0th-plane
   //bottom-to-top dynamic programming
3: for  $i = 1$  to  $N$  do
4:   for  $l = i - \lfloor t_{max}/b \rfloor$  to  $i - \lceil t_{min}/b \rceil$  &l  $\geq 0$  do
5:     if  $\sum_{m=l+1}^i \tilde{\phi}(m) \leq \epsilon$  then
6:       if  $K[l] > K[i] + 1$  then
7:          $K[i] = K[l] + 1$ ;  $D[i] = l$ ;
   //backtracking
8:  $i = N$ ;
9: while  $i > 0$  do
10:   $S(i) = true$ ;
11:   $i = D(i)$ ;

```

The optimization based on the integral of metric profile in Eq. (1) works very well in the general models as will be shown in the result section. Moreover, we can optionally insert some must-slicing plane heuristically. For some special cases that a general flat metric profile has some sharp changes, the integration may not exceed the allowable limit even a sharp change is included, because its neighborhood is very low in value. For instance, the CAD model shown in Fig. 4 has two such kind of sharp changes in the profile (marked as A and B) due to the transitions between the cube and the cylinder. Fortunately, the sharp changes can be easily detected in the profile, and thus the special case can be easily handled. We

introduce one more step before applying the optimization, and it is simply to go through the profile from the bottom to the top and compute the difference for each consecutive interval. If the difference is greater than a threshold (i.e., 0.5), a slice is placed in the upper interval, and the profile is separated into two segments by the slice. After that, the optimization can be performed separately in different segments, and they are assembled to a final result. Fig. 4 has shown the detail of this step.

3.4. Tool path/image generation

After obtaining the optimal slicing plan, we can generate the projection images for SLA printers, or the tool paths for FDM printers. Traditionally, the contours for the images are directly computed from the intersection between the z planes and the CAD model [34], which usually needs triangulation of the contour to generate the images. On the contrary, because LDI is a kind of ray representation, we can easily determine whether a certain pixel is black/white by checking the position of this pixel [35]. Specifically, given that the resolution of the image is the same as that of LDI in the z direction, for any height of an image plane, we can go through every ray of the LDI in each pixel and find the least sampling point that is greater than the given height. After that, the black/white of the pixel can be determined by the In/Out specification of the sampling point. As the sampling point is the next intersection point along the ray in the z direction, if it is specified as Out, then the position of the pixel has to be inside the model and the pixel should be white, and vice versa. This can generate the images in a very efficient way. The tool paths are then designed by the sequence for accumulating material to fill up the whole image.

4. Other factors

Our slicing pipeline is a general slicing framework based on sampling approach. In this section, we extend our adaptive slicing framework by considering other factors rather than cusp heights: (1) other commonly used error metrics are shown to be compatible with our framework, (2) the mesh saliency map is integrated into the metric profile to preserve the salient features, and (3) the proposed slicing algorithm can be served as a building block in searching the optimal fabrication direction efficiently.

4.1. Different metric profiles

In physical modeling, the commonly used geometry deviation error metrics includes cusp height, surface roughness, area deviation, volume deviation. We show that our framework is general to incorporate these metrics. Fig. 5 shows all the metric profiles and their corresponding slicing plans. We have already demonstrated our framework using cusp heights, and we will briefly describe the details of formulation for others below.

4.1.1. Surface roughness

Singhal et al. [8] figured out a statistic model for predicting the surface roughness (R_a), and the overall metric is the averaging surface roughness of the whole part,

$$R_a = \frac{t}{\sin \theta}, \quad (7)$$

where θ is the building angle between the building direction z and surface normal, and t is the layer thickness. Similar to the derivation of metric profile using cusp height in Section 3.1, surface roughness metric profile can be expressed as the derivative of surface roughness error:

$$\phi_{R_a}(z) = \frac{dR_a}{dz} = \lim_{\Delta z \rightarrow 0} \frac{\Delta R_a}{\Delta z} = \frac{1}{\sin \theta}, \quad (8)$$

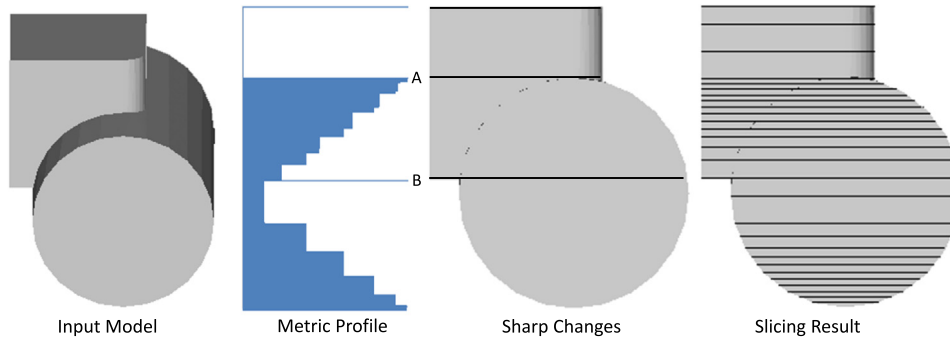


Fig. 4. Based on the metric profile of a given CAD model, sharp changes (located at A and B, which are the sharp transitions between the cube and the cylinder) can be detected. Our algorithm can successfully place slicing planes on these positions.

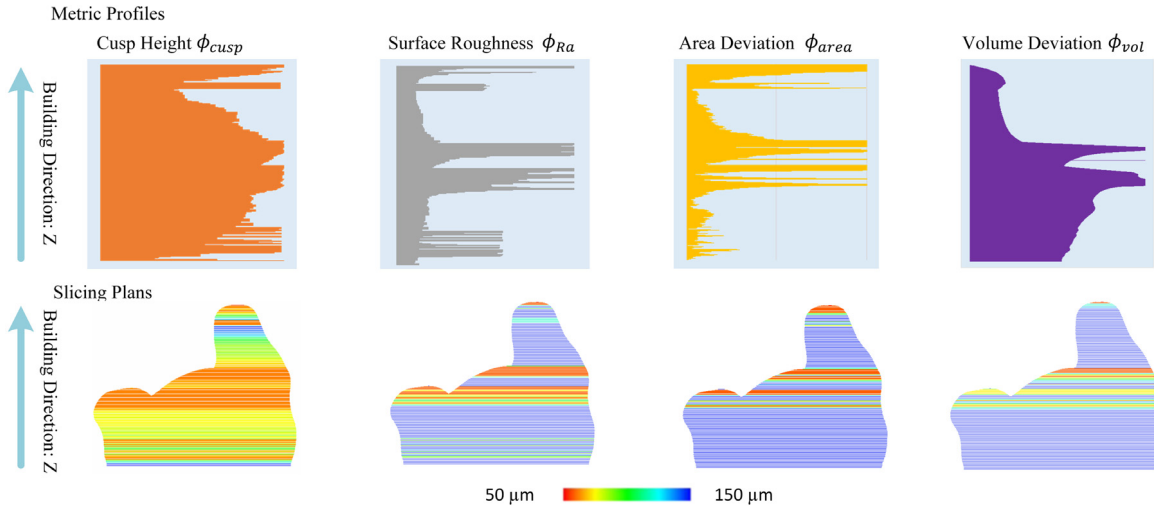


Fig. 5. Metric Profiles with different geometric error are shown in the top and the corresponding slicing plans are shown in the bottom. The colors in the slicing plan range from red to blue, indicating from the smallest thickness ($50 \mu\text{m}$) to the largest thickness ($150 \mu\text{m}$). (For interpretation of the references to color in this figure legend, the reader is referred to the web version of this article.)

where $\phi_{Ra}(z)$ returns the maximum value of $\sin^{-1} \theta$ for all the points at height z .

In the software implementation, given a sampled model $P = \{p_j\}$, we know the point coordinate (x_j, y_j, z_j) , and the normal (n_j^x, n_j^y, n_j^z) of each point j , and the angle θ between point normal and fabrication direction satisfies $\cos \theta = n_j^z$. Thus, the maximal surface roughness of the interval i can be computed as

$$\tilde{\phi}_{Ra}(i) = \max \left\{ \frac{1}{\sqrt{1 - n_j^z{}^2}} \mid \lceil z_j/b \rceil = i, p_j \in P \right\}. \quad (9)$$

Hence, the metric profile value for surface roughness at height z could be approximated as

$$\phi_{Ra}(z) \approx \tilde{\phi}_{Ra}(\lceil z/b \rceil). \quad (10)$$

4.1.2. Area deviation

Zhao [7] presented area deviation as a new surface quality metric for their adaptive slicing algorithms. The area deviation is defined as the relative deviation of top area and bottom area of a layer,

$$\delta_A = \frac{|A_{z_{k+1}} - A_{z_k}|}{A_{z_k}}. \quad (11)$$

We can obtain the area deviation profile for an infinitesimal layer thickness as

$$\phi_{area}(z) = \frac{d\delta_A}{dz} = \left| \frac{dA_z}{dz} \right| \frac{1}{A_z} = \frac{|A'_z|}{A_z}, \quad (12)$$

where A_z is the area of slicing at z plane, and A'_z is the derivative of A_z .

The computation of the area in a particular height z is similar to the image generation described in Section 3.4. The area of a layer is computed by the number of pixels that are specified as white in the image plane at the specific height, i.e. assuming there are N_w pixels are in white, the area is approximated as

$$A_z \approx N_w \cdot w^2, \quad (13)$$

where w is the size of the pixel.

We have also generated a series of intervals having exactly the same size of the metric profile's one for storing the areas in different heights $A_z = \{\tilde{A}(1), \dots, \tilde{A}(N)\}$. The height value used to compute the area for each interval is taken as the center of the interval. Thus the area deviation of the interval i can be computed as

$$\tilde{\phi}_{area}(i) = \frac{|\tilde{A}'|}{\tilde{A}(i)} = \frac{|\tilde{A}(i+1) - \tilde{A}(i)|}{b\tilde{A}(i)}. \quad (14)$$

4.1.3. Volume deviation

Instead of checking only one-dimensional slicing error (cusp height) or two-dimensional slicing error (area deviation), Kumar and Choudhury [21] proposed a ‘‘cusp volume’’ metric to quantify the three-dimensional error, which is the volume error between the CAD model and the printed part. The volume of the k th layer with the height range (z_{k-1}, z_k) in the CAD model can be calculated as $V_{CAD} = \int_{z_{k-1}}^{z_k} A_z dz$. The corresponding layer volume in the

printed part is an extrusion with its bottom area $A_{z_{k-1}}$, i.e., $V_{printed} = A_{z_{k-1}} \cdot t_k$. Hence, the volume deviation of the k th layer is

$$\begin{aligned} \delta_V &= V_{CAD} - V_{printed} \\ &= \int_{z_{k-1}}^{z_k} A_z dz - A_{z_{k-1}} \cdot t_k. \\ &= \int_{z_{k-1}}^{z_k} (A_z - A_{z_{k-1}}) dz. \end{aligned} \quad (15)$$

Rewriting it as a differential form for a particular height z in the k th layer gives that

$$\frac{d\delta_V(z)}{dz} = \frac{d}{dz} \int_{z_{k-1}}^z (A_z - A_{z_{k-1}}) dz = A_z - A_{z_{k-1}}. \quad (16)$$

However, as the volume deviation is a height-dependent error metric, we cannot directly define the above equation as the metric profile. This is because the term A_{z_k} is not an independent term, but a specific term for a particular layer. Fortunately, our optimization framework based on dynamic program can handle this nonlinear problem with only a little modification. By defining the volume deviation profile as

$$\phi_{vol}(z) = A_z, \quad (17)$$

the metric error of the k th layer can be computed as

$$\varepsilon_k = \int_{z_{k-1}}^{z_k} |\phi(z) - \phi(z_{k-1})| dz. \quad (18)$$

Replacing the error computation in Eq. (2) by this one, the slicing algorithm presented in Procedure 1 works exactly the same for the area deviation. The computation of the area A_z is the same as Eq. (13), and thus the discrete form for Eq. (17) is

$$\tilde{\phi}_{vol}(i) = \tilde{A}(i), \quad (19)$$

with

$$\tilde{\varepsilon}_k = \sum_{j=l+1}^i |\tilde{\phi}(j) - \tilde{\phi}(l+1)| \cdot b. \quad (20)$$

4.1.4. Comparing different error metric profiles

Fig. 5 compares metric profiles and slicing results of different error metrics. The metric profiles reflect the features of the users' interest. For example, the volume deviation metric cares about the portion that has a large amount of volume error, and the bottom half part has a large volume and thus the bottom half of error metric profile is larger than up half part's. In comparison, the cusp height metric measures the cusps which is not related to the contour size, and hence it has relatively balanced metric profile compared to the volume deviation metric profile.

The exemplary "hearing aid" model in Fig. 5 has surfaces facing up around the middle height. These surfaces introduce large staircase error. We also notice that all these error metric profiles have the largest error density value at the height of these surfaces. Accordingly, all the four optimal slicing results have a smaller layer thickness at the height of these surfaces, i.e. the red lines in the middle height.

Similar to the "cusp height" in Eq. (4), the error metrics "surface roughness" in Eq. (8) and "area deviation" in Eq. (12) are formulated as the integral of density function $\phi(z)$, which only depends on the particular height (z). Therefore, all the three error metrics have the "additive" property: the error for a thick layer is the sum of the errors evaluated on the thinner layers that are combined into the thicker layer. However, the formulation Eq. (18) indicates that this "additive" property does not hold for the volume deviation, because the error density function depends not only the information of height (z) but also the base height of that layer (z_{k-1}). Fortunately, the "volume deviation" for any layer can be easily computed using the Eq. (18), with underlying precomputed profile $\phi_{vol}(z) = A_z$.

4.2. Slicing of weighted CAD model

In some cases, the features of a CAD model are not equally important, and a straightforward idea is that the more salient features will be sliced with a smaller layer thickness. For example, in the CAD model of Fig. 6, the face of David model is considered as more salient than the rest part. By adding a weight (whose value ranges from 0 to 1) to each face, we can adjust the importance of each feature (face). In this paper, two methods of generating the weights are combined. Lee [36] introduced a multi-scale mesh saliency computation method, which is the basis of our salient mesh. We also develop an interactive interface for users to explicitly assign saliency level to each mesh facet or region. Then, a combined mesh weight map will be generated by the per-face product of geometry and user-specified saliency. An example can be found in Fig. 6. The saliency map for geometry-based method has high weight for small features along the z axis, while by specifying the high weight only in the face of David model, we can further focus our saliency weight onto the portion that the user prefers.

Recall that the LDI sampled points has the following information $P = \{p_j\} = \{x_j, y_j, z_j, n_j^x, n_j^y, n_j^z, f_j, r_j\}$. After each face has been assigned a weight value, each sampled point p_j can inherit the weight value from its belonged face. Denote each point's weight as $\omega(p_j)$. When computing the metric profile, each point's weight can be applied point-wisely to modify the metric profile. For example, the metric profile with "cusp height" considering weights is modified as

$$\phi_{cusp_w}(z) = \max \{n_j^z \cdot \omega(p_j) | z_j = z\}, \quad (21)$$

Similarly, the weighted metric profile with "surface roughness" is computed as

$$\phi_{Ra_w}(z) = \max \left\{ \frac{1}{\sqrt{1 - n_j^z^2}} \cdot \omega(p_j) | z_j = z \right\}. \quad (22)$$

However, metric profiles with "area deviation" and "volume deviation" are calculated using the area of the sliced contour at each height. We cannot apply the weight point-wisely for these two metric profiles. In this work, we conservatively pick the maximal weight at each height z to indicate the importance of that height. Then, the weighted metric profiles are formulated as

$$\phi_{area_w}(z) = \phi_{area}(z) \cdot \max \{\omega(p_j) | z_j = z\}, \quad (23)$$

$$\phi_{vol_w}(z) = \phi_{vol}(z) \cdot \max \{\omega(p_j) | z_j = z\}, \quad (24)$$

where $\phi_{area}(z)$ and $\phi_{vol}(z)$ refer to Eq. (12) and Eq. (17) respectively.

In the implementation, we also design a Graphic User Interface (GUI) to directly assign weights to selected faces of the CAD model in addition to the weights generated using the algorithm in Lee [36]. As the LDI sampled point provides the face ID it belongs to, we can retrieve the weight of the face. Thus, a weight map for all the features can be imported to our slicing algorithm, and the original metric profile "cusp height" will be adjusted as weighted metric profile with as shown in Fig. 7. After the weighted profile is computed, the rest of the slicing algorithm is exactly the same. Fig. 7 shows the optimal slicing plan of the weighted model.

The fabrication results demonstrate that the slicing with weight map has smoother surface on the David's face than the one without weight map. Comparing with the non-weighted CAD model, the weighted model has large weight values in the face region. Correspondingly, the weighted metric profile has a large value at the height of the face. Therefore, in the optimal slicing plans, the slicing result of weighted CAD model has smaller layer thickness (red lines) in the area of David's face. Eventually, this finer slicing yields a smoother David's face with finer layers, i.e. with smaller cusps and staircases.

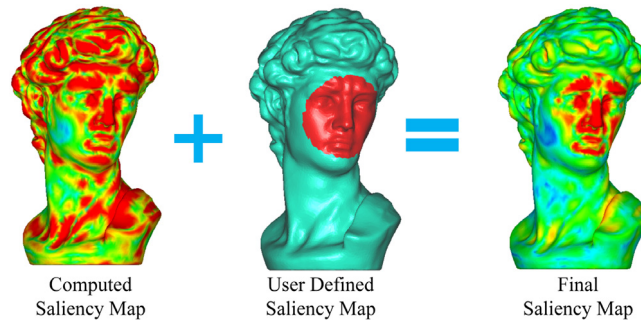


Fig. 6. CAD model with weighted surface, and the right salient map is a combination of geometry saliency map (left) and user-defined saliency map (middle).

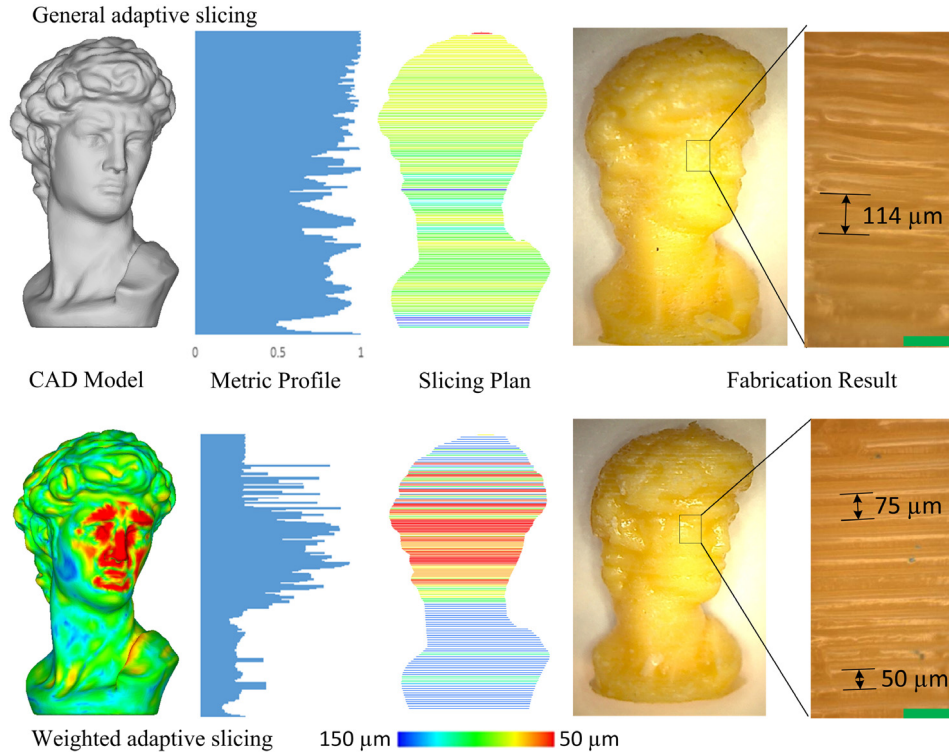


Fig. 7. Slicing comparison between weighted and non-weighted CAD model. The top part of the figure is a general slicing plan, which is almost uniform slicing, and the slicing in the bottom has small thicknesses in high weight positions. The colors in the slicing plan range from red to blue, indicating from the smallest thickness ($50 \mu\text{m}$) to the largest thickness ($150 \mu\text{m}$). The very right column shows the weighted result in bottom has smaller cusps, and the scale bar is $200 \mu\text{m}$. (For interpretation of the references to color in this figure legend, the reader is referred to the web version of this article.)

4.3. Building direction

Determining an optimal printing orientation can further improve the printing performance, and it can be based on different criterion, e.g., visual saliency [20], perceptual model [32], mechanical strength [37], etc. As will be demonstrated in the result section, our proposed slicing algorithm is very efficient that can complete the slicing plan for all the models within one second. Such efficiency plays an important role in finding the optimal fabrication orientation, which requires a large number of slicing evaluations along different orientations (normally about 1000 direction candidates).

In this paper, we present a nested loop to find the optimal building orientation based on the fabrication time and surface quality. In the outer loop, we uniformly sample the orientation space into 1000 directions (Fig. 8(a)). For each orientation, given the allowable maximum cusp height, we run our adaptive slicing algorithm as the inner loop, and obtain the optimal slicing plan with the corresponding fabrication time and surface quality.

We use the weighted summation of fabrication time and surface roughness as the objective energy function:

$$F(\mathbf{O}) = \alpha|K(\mathbf{O})| + (1 - \alpha)|\varepsilon(\mathbf{O})| \quad (25)$$

$|K(\mathbf{O})|$ is the number of layers at orientation \mathbf{O} , which is normalized by dividing the maximum of layer numbers over all orientations. $|\varepsilon(\mathbf{O})|$ is the geometric error at the orientation \mathbf{O} , which is also normalized by dividing the maximum geometric error over all orientations. The weighted ratio α is set as 0.5.

We use the “Pig” model as an example to show the usage of metric profile to find the optimal building orientation. This “Pig” model’s height is 58 mm. We uniformly sample the orientation space into 1000 directions (Fig. 8(a)). For each orientation, given the allowable maximum cusp height, we run our adaptive slicing algorithm, and obtain an optimal slicing plan and corresponding fabrication time and surface roughness. And the weighted objective energy is visualized in a Gaussian sphere as shown in Fig. 8(b,c), where the front-view and back-view of the Gaussian sphere are displayed with red and blue color represent large and

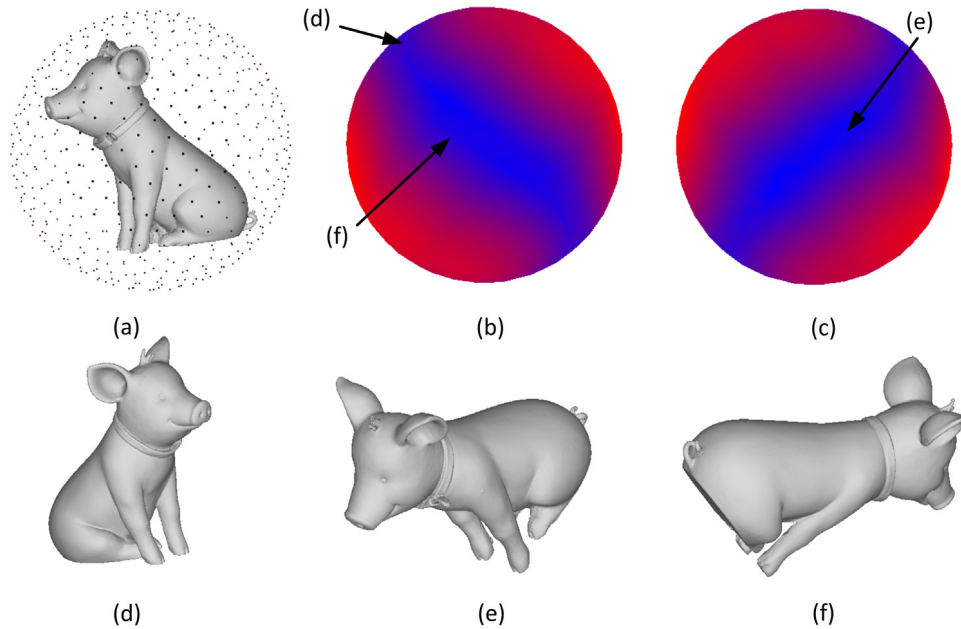


Fig. 8. (a) We uniformly sample the directions on a Gaussian sphere, and visualize the distribution of energy in a Gaussian sphere. Both the front view (b) and the back view (c) are displayed. The three best building orientations are shown in (d), (e), and (f).

small energy respectively. Three local best fabrication directions are identified as (d)(e)(f) in Fig. 8.

5. Result

Our slicing pipeline is implemented in C++, built on the open source package LDI [38]. All tests are run by a PC with Intel(R) Core(TM) i5-3450 CPU @3.10 GHz, 12GB RAM, and NVIDIA GeForce GT 640. The LDI sampling resolution is set as 2048. The heights of all the tested CAD models range from 17.8 mm to 62.4 mm. All the fabrication results are built using the SLA process [39]. We modified a Projet 1000 printer from 3D Systems to function with different layer thickness. The layer thickness is controlled by a Z-stage, and the practical thickness for a layer is from $t_{min} = 50 \mu\text{m}$ (0.002 inch) to $t_{max} = 150 \mu\text{m}$ (0.006 inch). The photo curing time of one single layer varies from 1 to 2 s respectively, while the overhead of transition between layers takes around 14 s.

Our implementation subdivides the metric profile into intervals with size b . Intuitively, the value of b should not be greater than the minimum layer thickness t_{min} that can be printed (i.e., $b \leq t_{min}$), otherwise the algorithm cannot optimize the position of the layers with minimum thickness; as an approximation, it is also preferred that b should be as small as possible to minimize information loss due to discretization. To determine a practical value of b , we have conducted an experiment on a “Hand” model with different b values and listed the results in Table 1. Without surprise, the computational time increases with the number of intervals (i.e., decrease in the b value), but the number of layers required to achieve the same quality is also decreased due to better approximation. For a balance between quality and speed, $b = 2 \mu\text{m}$ is selected in this paper.

5.1. Slicing efficiency

Table 2 compares the slicing software time of our adaptive slicing (T_{our}) with other slicing methods, including uniform slicing with both coarsest ($T_{co.}$) and finest (T_{fine}) layer thickness, local greedy adaptive slicing ($T_{loc.}$) introduced in paper [3], and the global slicing using ultra fine resolution (T_{ultra}), i.e. our sampling

Table 1
Sensitivity test of parameter b (the size of each interval)

b (μm)	50	25	10	5	2	1
$\lceil t_{min}/b \rceil$	1	2	5	10	25	50
#Intervals	475	950	2377	4754	11885	23771
Time (ms)	0	1	1	2	20	173
#Layers	∞	∞	246	239	234	232

Different b values are tested. #Intervals – the number of intervals that the metric profile is discretized into, $\lceil t_{min}/b \rceil$ shows how many intervals the minimum layer thickness contains. “Time” – the running time of our algorithm, and the time unit is ms . #Layers – the resulted number of layers, and ∞ means there is no feasible solution.

Table 2
Slicing efficiency comparison.

Input	#Tri	#L	T_{our}	$T_{co.}$	$T_{loc.}$	T_{fine}	T_{ultra}
Glass1	30K	515	0.62	4.8	10.7	14.4	148.2
Glass2	30K	344	0.72	5.2	10.3	15.4	160.3
Knee	39K	625	0.58	10.3	19.1	30.8	328.7
Hand	84K	233	0.53	15.8	24.4	47.6	377.3
HearAid	33K	286	0.81	3.5	7.0	10.4	140.8

The time units are in seconds. #Tri is the number of triangles in each STL model. #L is the number of layers by our slicing algorithm. T_{our} , $T_{co.}$, $T_{loc.}$, T_{fine} , T_{ultra} represent slicing time of our algorithm, coarsest uniform, local greedy, finest uniform, ultra resolution slicing.

resolution ($t = 12.5 \mu\text{m}$), is much smaller than the finest layer thickness ($t = 50 \mu\text{m}$).

From the slicing results, our new pipeline consumes less than 1 s in total including sampling, constructing profile, generating and optimizing the slicing plan. In contrast, the direct slicing algorithms need around 5 s for coarsest layer thickness and 15 s for finest layer thickness. It is worth reminding that the slicing time for the local greedy adaptive slicing algorithm [3] is only one single evaluation of a slicing plan, but our adaptive slicing algorithm evaluates all the possible slicing plans with the ultra fine resolution and outputs the global optimal one. For comparison, we have also shown the needed time for slicing plan optimization that is directly computed on the CAD model using the ultra fine resolution, denoted as T_{ultra} in Table 2. On average, our algorithm could achieve 100 times faster than the direct slicing. The effect is more significant when a large number of slicing will be performed

to optimize the fabrication orientation. In our orientation optimization experiment, it takes us less than 15 min to search among 1000 directions, while the slicing method directly computed on the CAD model needs more than 1 day.

5.2. Slicing quality

In Table 3, we compare our method with other slicing algorithms, including slicing methods using uniform layer thickness and a greedy adaptive slicing method proposed in [3]. The error metric used in Table 3 is “Cusp Height”. The left part of Table 3 shows the number of layers in the results computed by different slicing algorithms. It also reflects the printing time as the printing time is almost proportional to the number of layers. The right part of Table 3 shows the geometry error computed by the maximum error among all layers, i.e. $\max\{\epsilon_k\}$. Here, the cusp height is used as the error metric, and thus, this geometric error is also the maximum cusp height among all layers. Without any surprise, the coarsest uniform slicing always gives the smallest number of layers but has the largest geometric error, and the finest one always has the smallest geometric error but gives the largest number of layers. They are used as the upper bound and the lower bound for comparing the adaptive slicing algorithms.

Both of our proposed and the greedy [3] adaptive slicing algorithm have set the allowable geometric error as the cusp height of $\epsilon = 65 \mu\text{m}$ for one layer. From the table, we can see that the two methods fall right inside the upper and the lower bound in terms of the layer number and geometric error. The results verify that both of the methods are effective. However, our algorithm can achieve a smaller number of layers under the same tolerance, and thus a smaller printing time (save up to 16% printing time). Moreover, due to the geometric complexity of the model and the fabrication constraints, the greedy algorithm fails to distribute the errors evenly on the layers. Hence their results are not optimal, and even cannot always satisfy the given tolerance for all the layers. In contrast, our algorithm has a global information for the planning, and our results can successfully satisfy the given tolerance in all cases. Last but not least, it is found that our adaptive slicing can get very competitive results with the finest slicing, but our results have much fewer number of layers and can save up to 49% printing time. It validates our proposed method is not only efficient but also promising.

5.3. Other examples and fabrication results

We have applied our adaptive slicing algorithm using “Cusp Height” error metric on various models as shown in Fig. 9. These slicing results reveal an intuition that the layer thickness gets smaller at the height with increased geometry error density (i.e. with a larger value in the metric profile). This intuition results from the error constraint in each layer in Eq. (2), that is the error of each layer cannot exceed the limit ϵ . Hence, if the error density of a layer is large, then the layer thickness should be small so that the total integral error in the layer does not exceed the limit ϵ .

Fig. 10 displays the physical fabrication results using different slicing algorithms. From the microscope images (the bottom row of Fig. 10), we can see that the results from our slicing algorithm using “Cusp Height” error metric is very close to the one produced by the slicing with the finest layer thickness (the very left image in Fig. 10). Comparing with the results of the uniform slicing and local adaptive slicing, our result has a better surface finish, i.e. our result has less noticeable cusps and staircases. Fig. 11 is another example to validate our slicing method. Similar to Fig. 10, the result using our method has fewer staircase defects comparing with other slicing algorithms like greedy and uniform slicing.

6. Conclusion and discussion

This paper presents a novel adaptive slicing algorithm for the layer-based additive manufacturing. Traditional adaptive slicing algorithms suffer from long computation time or yield sub-optimal slicing result based on local geometry error. To generate the global optimal slicing plan efficiently, we introduce a novel algorithm based on a “metric profile”, which is a measure of geometry error distribution along a given building direction. The efficiency and effectiveness of our algorithm are enabled by three key ideas in our paper: (1) the new representation of metric profile provides us the global geometry deviation along the z direction, rather than only geometry error on the slicing planes that are used in most traditional methods, (2) we efficiently construct the metric profile using a GPU-accelerated sampling approach, and (3) an optimization algorithm based on dynamic programming is proposed to find the global optimal slicing plan efficiently. Such advantages have been validated by comparing the computational time and fabrication quality with other slicing algorithms.

Our slicing method is a general adaptive slicing framework, and we have extended it to consider weighted features of a CAD model and to incorporate the commonly used surface quality metrics, such as cusp height, surface roughness, area deviation, and volume deviation. Our slicing algorithm can also serve as a building block for computing the optimal printing direction.

Our future works will be applying this framework to other geometric computation tasks that are required in the pre-fabrication pipeline of AM processes, and to speed up the process planning for AM applications like mass customization.

Acknowledgments

The work is partially supported by National Science Foundation (NSF) grant number CMMI 1151191 and the Epstein Institute at University of Southern California.

Appendix. Approximation errors analysis

To determine a new slicing plane efficiently, the conventional slicing algorithm usually considers the normal of the intersection points by the previous slicing plane. In other words, it uses the normal to linearly approximate the surface between the two slicing planes, and uses the cusp height to determine the slicing error. When the layer thickness is small or the true surface is close to linear, such as the one shown in Fig. A.1(a), the cusp height is a good estimation of the approximation error during slicing and is widely used. However, such simplification can lead to inaccurate estimation when the surface is highly curved and a layer of fabrication becomes much thicker.

Before the analysis, the terminologies are defined first for clarification. The “true geometry” refers to the designed CAD model; “printed geometry” refers to the physical geometry created by the printer, shown as the solid blue portion in Fig. A.1.; “approximated geometry” indicates the estimated printed-geometry using the error metric before the physical printing, e.g., the geometry enclosed by the dashed line in Fig. A.1. Correspondingly, the “true slicing error” means the geometry discrepancy between the true geometry and the printed geometry; and the “approximated error” means the geometry discrepancy between the approximated geometry and the printed geometry.

The idea of our proposed metric profile is illustrated in Fig. A.1(b) using three smaller layers. The cusp heights are calculated separately in each small layer, and they are integrated as the error for the whole layer. In this case, the proposed integral error metric just recovers the cusp height of the thick layer as the big layer’ cusp height is the sum of three small layers’ ones.

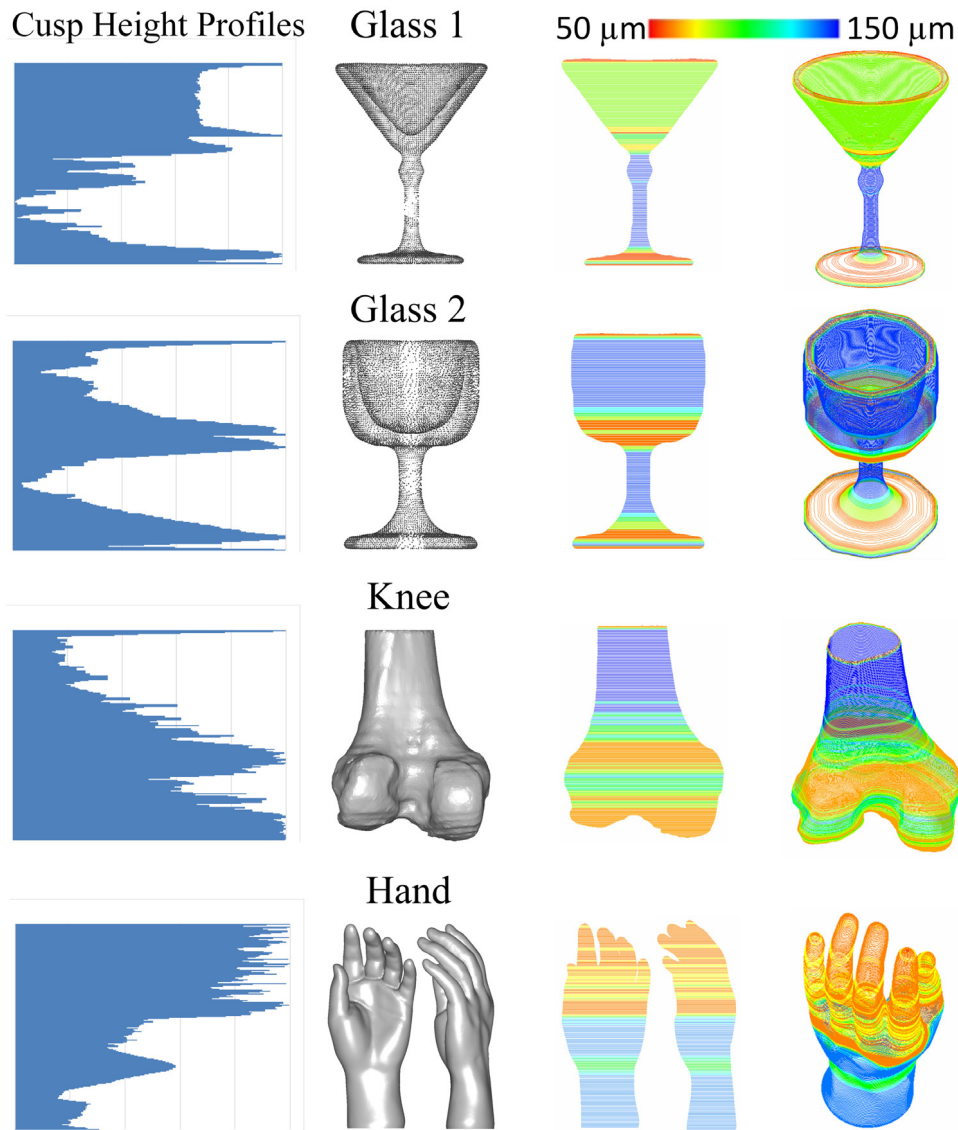


Fig. 9. Adaptive slicing results of various models.

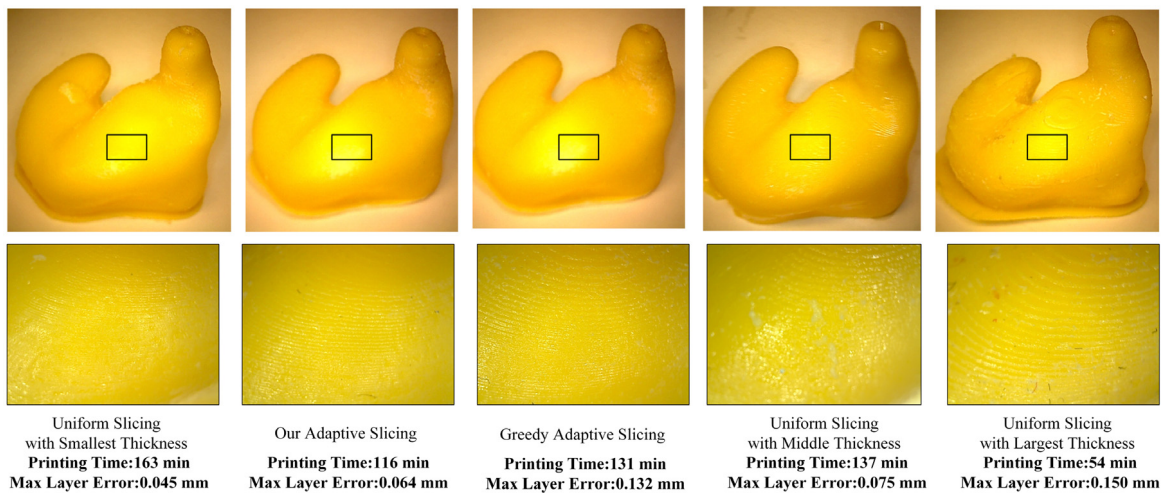


Fig. 10. Fabrication results of hearing aid model by different slicing methods.

Table 3
Slicing performance comparison with other slicing algorithms.

Input model		Number of layers					Geometric error (mm)			
Name	Height	#Tri	Coarsest	Our	Greedy	Finest	Coarsest	Our	Greedy	Finest
David	17.8	42K	117	237	272	350	0.151	0.065	0.077	0.050
HearAid	22.3	33K	147	286	358	440	0.152	0.065	0.136	0.050
Hand	23.8	84K	156	233	255	468	0.149	0.065	0.084	0.049
Laurana	37.4	51K	245	466	556	736	0.152	0.065	0.114	0.050
Glass2	39.0	30K	256	344	376	768	0.152	0.065	0.082	0.050
Glass1	55.1	30K	362	515	576	1085	0.152	0.065	0.093	0.050
Pig	58.0	729K	382	747	917	1145	0.152	0.065	0.910	0.050
Knee	62.4	39K	410	625	715	1229	0.152	0.065	0.084	0.050

† We compare our method with the finest uniform slicing, greedy adaptive slicing [3], and coarsest uniform slicing, denoted as “Finest”, “Greedy” and “Coarsest” in the table. A set of models with various heights are sliced, and the results are compared in terms of the number of layers (the middle part of the table) and the geometric error (maximum layer’s integral error among all layers, unit: mm, the right part of the table). The height unit is mm, #Tri means the number of triangles in each STL model, and the geometric error uses the metric “Cusp Height”.

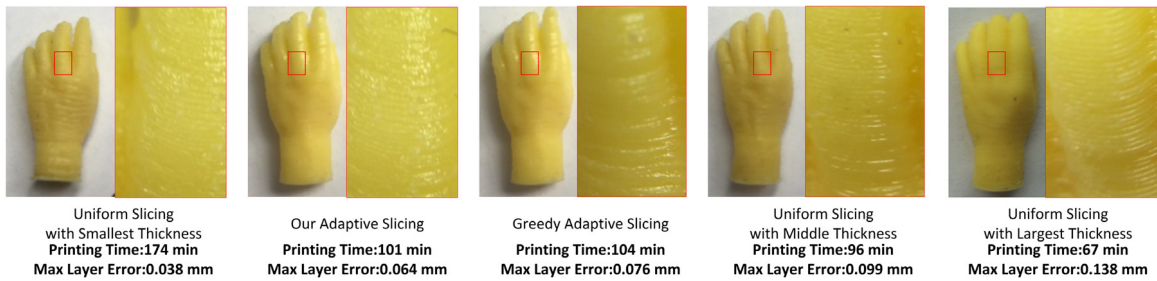


Fig. 11. Fabrication results of hand model by different slicing methods.

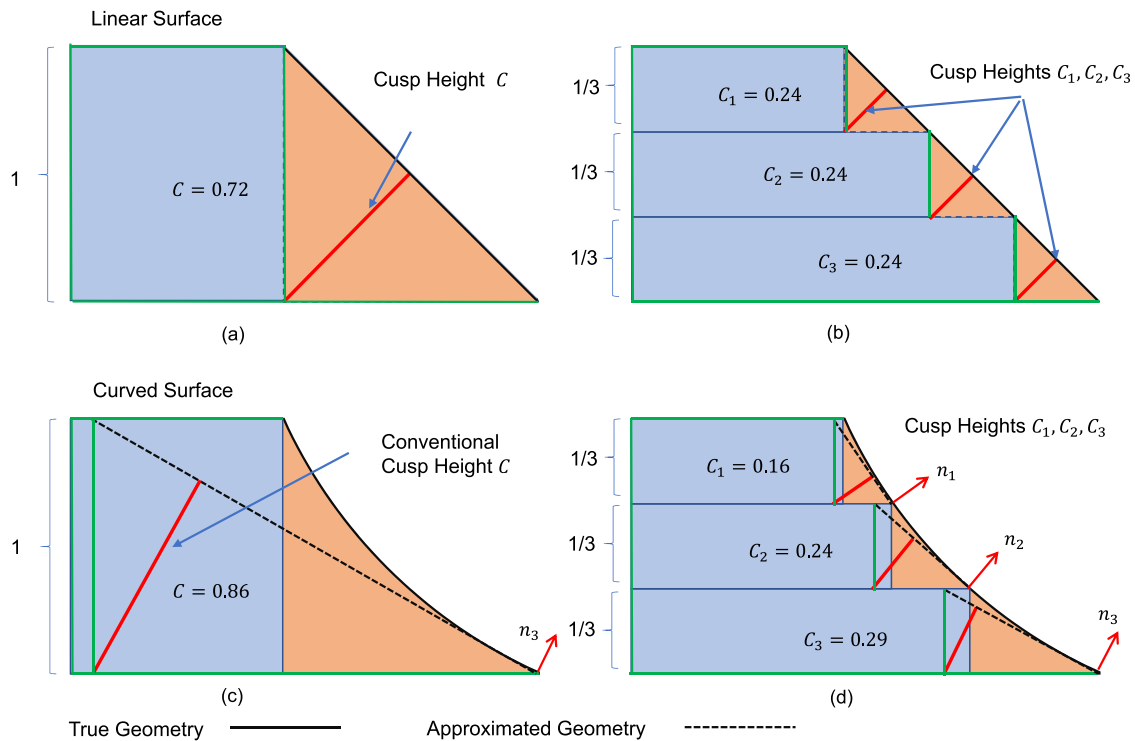


Fig. A.1. (a) and (c) illustrate the conventional method of approximating the printed geometry using cusp height; (b) and (d) are the proposed method for the approximation. The true geometry in the top row is a line, and the bottom row is a concave curve. The printed shapes are the extruded rectangles.

Nevertheless, when the true surface is not linear, simply considering the normal of the previous plane results in a poor approximated surface and inaccurate error estimation. For example, if the bottom plane’s normal is used for the curve shown in Fig. A.1(c), the approximated surface is outlined by the dotted line. The true slicing error for this curve surface should be similar to (probably

a bit smaller than) the one shown in Fig. A.1(a), because the true geometry in Fig. A.1(c) is a slightly concave shape of the one in Fig. A.1(a). Unfortunately, because the approximated geometry is different from the true geometry and the conventional method only takes a single normal vector, but the actual curved surface

has many different normal vectors, the slicing error is computed as 0.86, which is much higher than the linear one 0.72.

In comparison, our error metric profile records the normal at each height, illustrated in Fig. A.1(d) using three small layers again. The cusp height of each layer is calculated using the normal in its own height. The sum of three small layer's cusp height is $0.16 + 0.24 + 0.29 = 0.69$, which is a bit smaller than 0.72 calculated from the similar linear curve. If we further divide the smaller layers, an even better approximation will be obtained. When the small layers are infinitesimal, this calculation converges to the error obtained by integrating the error metric profile.

References

- [1] Freedman DH. Layer by layer. *Technol Rev* 2012;115(1):50–3.
- [2] Gibson I, Rosen DW, Stucker B. Additive manufacturing technologies: rapid prototyping to direct digital manufacturing. first edition. Springer; 2009.
- [3] Dolenc A, Mäkelä I. Slicing procedures for layered manufacturing techniques. *Comput Aided Des* 1994;26(2):119–26.
- [4] Kulkarni P, Dutta D. An accurate slicing procedure for layered manufacturing. *Comput Aided Des* 1996;28(9):683–97.
- [5] Hayasi MT, Asiabanpour B. A new adaptive slicing approach for the fully dense freeform fabrication (fdff) process. *J Intell Manuf* 2013;24(4):683–94.
- [6] Ma W, But W, He P. NURBS-based adaptive slicing for efficient rapid prototyping. *Comput Aided Des* 2004;36(13):1309–25.
- [7] Zhao Z, Laperrière L. Adaptive direct slicing of the solid model for rapid prototyping. *Int J Prod Res* 2000;38(1):69–83.
- [8] Singhal S, Jain PK, Pandey PM. Adaptive slicing for SLS prototyping. *Comput Aided Design Appl* 2008;5(1–4):412–23.
- [9] Li L, Kochhar AK, Liu W. Mathematical modelling of geometrical error transformation process in additive rapid prototyping/manufacturing. In: The 7th European conference on rapid prototyping and manufacturing, Aachen; 1998.
- [10] Ancau M. The optimization of surface quality in rapid prototyping processes. The Free Library; 2009.
- [11] Kulkarni P, Marsan A, Dutta D. A review of process planning techniques in layered manufacturing. *Rapid Prototyp J* 2000;6(1):18–35.
- [12] Mohan Pandey P, Venkata Reddy N, Dhande SG. Slicing procedures in layered manufacturing: a review. *Rapid Prototyp J* 2003;9(5):274–88.
- [13] Yang P, Qian X. Adaptive slicing of moving least squares surfaces: toward direct manufacturing of point set surfaces. *J Comput Inf Sci Eng* 2008;8(3):031003–11.
- [14] Yang P, Li K, Qian X. Topologically enhanced slicing of MLS surfaces. *J Comput Inf Sci Eng* 2011;11(3):031003–9.
- [15] Xu F, Wong Y, Loh H, Fuh J, Miyazawa T. Optimal orientation with variable slicing in stereolithography. *Rapid Prototyp J* 1997;3(3):76–88.
- [16] Cormier D, Unnanon K, Sanii E. Specifying non-uniform cusp heights as a potential aid for adaptive slicing. *Rapid Prototyp J* 2000;6(3):204–12.
- [17] Jung JY, Ahluwalia RS. NC tool path generation for 5-axis machining of free formed surfaces. *J Intell Manuf* 2005;16(1):115–27.
- [18] S. Pande S, Kumar S. A generative process planning system for parts produced by rapid prototyping. *Int J Prod Res* 2008;46(22):6431–60.
- [19] Liu S, Wang CCL. Duplex fitting of zero-level and offset surfaces. *Comput Aided Des* 2009;41(4):268–81.
- [20] Wang W, Chao H, Tong J, Yang Z, Tong X, Li H, Liu X, Liu L. Saliency-Preserving slicing optimization for effective 3D printing. *Comput Graph Forum* 2015;34(6):148–60.
- [21] Kumar C, Choudhury AR. Volume deviation in direct slicing. *Rapid Prototyp J* 2005;11(3):174–84.
- [22] Chang C. Direct slicing and g-code contour for rapid prototyping machine of uv resin spray using powersolution macro commands. *Int. J Adv Manuf Tech* 2004;23(5–6):358–65.
- [23] Huang P, Wang CC, Chen Y. Intersection-free and topologically faithful slicing of implicit solid. *J Comput Inf Sci Eng* 2013;13(2):021009.
- [24] Zhou C, Chen Y, Yang Z, Khoshnevis B. Digital material fabrication using mask image projection based stereolithography. *Rapid Prototyp J* 2013;19(3):153–65.
- [25] Chen Y, Wang CCL. Layer depth-normal images for complex geometries: part one—accurate modeling and adaptive sampling. In: ASME international design engineering technical conferences and computers and information in engineering conference. ASME; 2008, p. 717–28.
- [26] Wang CCL, Chen Y. Layered depth-normal images for complex geometries: part two manifold preserved adaptive contouring. In: ASME international design engineering technical conferences and computers and information in engineering conference. ASME; 2008, p. 729–39.
- [27] Kwok T, Chen Y, Wang CCL. Geometric analysis and computation using layered depth-normal images for three-dimensional microfabrication. In: Three-dimensional microfabrication using two-photon polymerization. Oxford: William Andrew Publishing; 2016, p. 119–47. <http://dx.doi.org/10.1016/B978-0-323-35321-2.00007-8>.
- [28] Chen Y, Wang CCL. Uniform offsetting of polygonal model based on layered depth-normal images. *Comput Aided Des* 2011;43(1):31–46.
- [29] Wang CCL, Manocha D. GPU-based offset surface computation using point samples. *Comput Aided Des* 2013;45(2):321–30.
- [30] Wang CCL, Leung Y, Chen Y. Solid modeling of polyhedral objects by layered depth-normal images on the gpu. *Comput Aided Des* 2010;42(6):535–44.
- [31] Chen Y, Wang CCL. Regulating complex geometries using layered depth-normal images for rapid prototyping and manufacturing. *Rapid Prototyp J* 2013;19(4):253–68.
- [32] Zhang X, Le X, Panotopoulou A, Whiting E, Wang CCL. Perceptual models of preference in 3D printing direction. *ACM Trans Graph* 2015;34(6):215:1–215:12.
- [33] Kleinberg J, Tardos É. Algorithm design. Pearson Education India; 2006.
- [34] Zhang Z, Joshi S. An improved slicing algorithm with efficient contour construction using stl files. *Int J Adv Manuf Tech* 2015;80(5–8):1347–62.
- [35] Huang P, Wang CCL, Chen Y. Algorithms for layered manufacturing in image space. ASME Press; 2014.
- [36] Lee CH, Varshney A, Jacobs DW. Mesh saliency. *ACM Trans Graph* 2005;24(3):659–66.
- [37] Umetani N, Schmidt R. Cross-sectional structural analysis for 3D printing optimization. *SIGGRAPH Asia* 2013;5:1–4.
- [38] LDNI-based solid modeling. <https://sourceforge.net/projects/ldnibasedsolidmodeling/>. [Accessed 4 September 2016].
- [39] Pan Y, Zhou C, Chen Y. A fast mask projection stereolithography process for fabricating digital models in minutes. *J Manuf Sci Eng* 2012;134(5):051011.